PCCP

ROYAL SOCIETY OF CHEMISTRY

PAPER

View Article Online
View Journal | View Issue

Cite this: *Phys. Chem. Chem. Phys.*, 2022, **24**, 20400

First-principles insights into hydrogen trapping in interstitial-vacancy complexes in vanadium carbide

Shuai Tang,*[a] Lin-xian Li,[a] Qing Peng,*[b] Hai-le Yan,[c] Ming-hui Cai,[ad] Jian-ping Li,[a] Zhen-yu Liu[a] and Guo-dong Wang[a]

Received 28th May 2022,
Accepted 5th August 2022

DOI: 10.1039/d2cp02425j

rsc.li/pccp

Hydrogen trapping is a key factor in designing advanced vanadium alloys and steels, where the influence of carbon vacancies is still elusive. Herein we have investigated the effect of carbon vacancies on the hydrogen trapping of defect-complexes in vanadium carbide using first-principles calculations. When a carbon vacancy is present, the second nearest neighboring trigonal interstitial is a stable hydrogen trapping site. A C vacancy enhances the hydrogen trapping ability by reducing the chemical and mechanical effects on H atom solution energy. Electronic structure analysis shows that C vacancies increase the charge density and the Bader atomic volume, leading to a lower H atom solution energy. The strength of the V–H bond is predominant in determining the hydrogen trapping ability in the presence of a C vacancy, in contrast to that of a C–H bond when the C vacancy is absent.

1. Introduction

With excellent high temperature mechanical properties and low activation characteristics under neutron irradiation conditions, vanadium alloys and reduced activation ferritic/martensitic steels have promising applications as structural materials in fusion reactors.[1,2] However, the penetration of a large amount of hydrogen and its isotopes in the fusion reactor service environment induces hydrogen embrittlement (HE) and degradation of materials, shortening the lifetime and causing safety issues.[3–7] It is known that the diffusion of H atoms is the leading cause of HE.[8–10] The use of hydrogen permeation barrier coatings that reduce the penetration of H is an effective means.[11,12] Among them, VC is valued for its high hardness and thermal stability, which not only improves the wear resistance of the material,[13,14] but also acts as an effective barrier to hydrogen permeation.[15]

The solubility of H atoms in VC traps is generally higher than in other traps, which significantly reduces the occurrence of HE.[16–21] Tetrahedral interstitial, trigonal interstitial and vacancies in VC crystals are often regarded as irreversible hydrogen traps. However, it is hard to directly quantify the trapping capabilities of traps by experiments, such as electron microscopy and thermal desorption spectroscopy.[22–24] Through Density Functional Theory (DFT) calculations, the effect of interstitial defects on the material's structural stability and bonding properties can be calculated.[25,26] In particular, the analysis of the H atom solution energy of trapping sites can elucidate the characteristics of the hydrogen traps.[27,28] It is reported that compared to the tetrahedral interstitial site, the H atom solution energy at the trigonal interstitial site in a perfect VC crystal is lower and more stable.[29] The intrinsic point defects including carbon vacancies are inevitable in a real crystal VC[30–32] due to thermal equilibrium at finite temperatures. The H atom solution energy of a C vacancy is the lowest among all the sites, suggesting that the C vacancy is the most stable hydrogen trapping site.[33,34] Nevertheless, the hydrogen trapping behavior has been considered only for the condition of the single site in the above studies, while that of the complex sites has rarely been considered. But it contributes to understanding the strong binding effect of the C vacancy on hydrogen. Therefore, it is essential to construct a VC crystal structure including C vacancies and study the H atom solution energy of sites neighboring C vacancies. It helps to elucidate the hydrogen trapping behavior under the combined effects of different sites around defect-complexes.

An in-depth study of the hydrogen trapping mechanism reveals the direct influence of H atoms on the structure of carbide. It is also essential to understand the interaction between the hydrogen and vacancy in the HE mechanism (hydrogen-enhanced strain-induced vacancy theory). Numerous studies have

[a] State Key Lab of Rolling and Automation, Northeastern University, Shenyang 110819, China. E-mail: tangshuai@ral.neu.edu.cn
[b] State Key Laboratory of Nonlinear Mechanics, Institute of Mechanics, Chinese Academy of Sciences, Beijing 100190, China. E-mail: pengqing@imech.ac.cn
[c] School of Materials Science and Engineering, Northeastern University, Shenyang 110819, China
[d] Key Lab of Lightweight Structural Materials, Liaoning Province, Northeastern University, Shenyang, 110819, China

suggested that the charge density distribution and the strength of the interaction between the H atom and neighboring atoms play a crucial role in determining the hydrogen trapping ability of stable sites. Regarding pure metals, Xing[35] found that H atoms prefer to occupy higher charge density interstitial sites, and the maximum number of trapped H atoms correlates with the decrease in the stability of the hydrogen-vacancy complex due to the charge transfer. Liu[36] suggested that H atoms tend to occupy the optimal charge density surface around a vacancy. Furthermore, as the number of H atoms increases, the optimal charge density surface area available for H atoms to occupy will decrease. Su[37] believed that at least 27-vacancy clusters are required to form stable H molecules due to the weak attraction between H atoms in vanadium. The above studies discuss the mechanism of hydrogen in pure metals, where the charge mechanism can be well adapted to pure metals due to the relatively simple chemical environment at the trapping site. However, the chemical environment of carbides is very complex,[38,39] where covalent, ionic, and metallic bonds could be present simultaneously. The applicability of this mechanism in carbides is worthy of further discussion. Wang[40] found that the strong bonding characteristics of the C–H bond may be necessary for the stability of the H atom. When a Zr vacancy exists in ZrC, it is difficult to trap the H atom at the Zr vacancy due to the weak C–H bonding with neighboring C atoms.[41] Huang[42] suggested that in the V_xC_y phase (VC, V_2C, V_4C_3, V_6C_5, and V_8C_7), the greater the number or strength of the bonding peaks generated by the hybridization of H with V and C atoms, the stronger the stability of hydrogen. This indicated that the H is subjected to the combined effect of neighboring metal (M) and carbon (C) atoms at the trapping site.

Despite previous efforts, the question of why H atoms interact with neighboring atoms to affect the hydrogen trapping ability of stable sites is still not well answered. It is required to quantitatively evaluate the bonds between H and neighboring atoms in different chemical environments. In this work, the hydrogen trapping ability of stable sites, including the neighboring sites of C vacancies in VC, was quantified by DFT calculations, and the chemical and mechanical effects of H atom solution energy were discussed. The electronic structures of the stable hydrogen trapping sites were quantitatively analyzed, and the relevant electronic structure parameters that can be used to evaluate the hydrogen trapping ability of the sites in different chemical environments were proposed. In addition, the bonding characteristics of H atoms occupying stable sites and surrounding atoms were quantitatively analyzed by the density of states (DOS) and crystal orbital Hamiltonian population (COHP).

2. Theoretical methods

The DFT calculations using the Vienna *ab initio* simulation package (VASP)[43] were performed in this study. The electron interactions with ions were replaced by the projector augmented wave (PAW)[44] method, and exchange–correlation potentials between electrons were parameterized by the generalized gradient approximation (GGA)[45] with the Perdew–Burke–Ernzerhof (PBE)[46] function. The $3p^6 3d^4 4s^1$ and $2s^2 2p^2$ electrons are the valence electrons of V and C, respectively. All calculations were based on a $3 \times 3 \times 3$ VC supercell, which contained 216 atoms without defects. When the structure was optimized, the atomic position and cell size were allowed to relax. The plane-wave cutoff energy was specified as 400 eV, and a $6 \times 6 \times 6$ *k*-point mesh obtained by the Monkhorst–Pack method was employed to sample the Brillouin zone.[47] The *k*-spacing is 0.014 $Å^{-1}$. The energy and atomic force convergence standard were set to 10^{-5} eV per atom and 0.03 eV per Å, respectively. Since zero-point energy corrections have little effect on the relative difference of energy, the zero-point energy corrections were not considered.[48] In this work, the charge density and crystal structures were graphically represented by VESTA.[49] The code developed by Henkelman's team[50] was utilized in the Bader charge analysis, and the COHP method in LOBSTER[51] was used to analyze the chemical bond.

The defect formation energy of the vacancy (E_f^{Vac}) can quantify the difficulty of vacancy formation, which is defined as:

$$E_f^{Vac} = E(VC + Vac) - E(VC) + \mu_i \quad (1)$$

where E(VC + Vac) and E(VC) are the energies of the VC supercell including a vacancy and VC supercell. μ_i is the average atomic energy of each substance in the pure elemental state, where C is graphite and V is bcc vanadium. The average atomic energy is obtained by dividing the total energy of the system with N atoms by the number of atoms N.

It is known that H atoms can occupy interstitial sites, vacancies and other sites of VC. The H atom solution energy (E^H) is used to evaluate the stability of H atoms at different sites, which is defined as:

$$E^H = E(\text{system} + H) - E(\text{system}) + 1/2E(H_2) \quad (2)$$

where E(system) and E(system + H) are the energies obtained by optimizing the atomic positions for a given VC system with or without defects and that containing a H atom. $E(H_2)$ is the energy of an H molecule in vacuum.

The H atom solution energy at different trapping sites can be divided into mechanical (E^{mech}) and chemical (E^{chem}) effects which are defined as:[52–56]

$$E^{mech} = E^{unrelax}(\text{system}) - E(\text{system}) \quad (3)$$

$$E^{chem} = E(\text{system} + H) - E_{unrelax}(\text{system}) + 1/2E(H_2) \quad (4)$$

where $E^{unrelax}$(system) is the energy after removing the H atom of a given VC system, which is obtained by fixing the atom of the VC system with the H atom removed and performing self-consistent calculations. The mechanical effect is the contribution of the local relaxation generated when H atoms occupy different trapping sites to the solution energy. The chemical effect is the contribution of the local chemical environment where H atoms occupy different trapping sites to the solution energy.

3. Results and discussion

3.1 Atomic structures

VC has a NaCl-type structure with the crystal structure shown in Fig. 1(a), in which the space group is $Fm\bar{3}m$. The calculated lattice parameter of VC is 4.150 Å, which is consistent with the experimental data[57] and the results of other calculated results.[58,59] The crystal structures of VC including a C or V vacancy are shown in Fig. 1(b and c), and their corresponding defect formation energy is shown in Table 1. The defect formation energy of the C and V vacancy is −0.915 eV and 4.507 eV, respectively, consisting of the computational result of Guo *et al.*[60] A negative (positive) defect formation energy indicates that the formation of the defect is exothermic (endothermic). The defect formation energy E_f^{Vac} determines the concentration of the defect C in a system under thermodynamic equilibrium at finite temperature T according to the Boltzmann distribution $C\tilde{e}^{-E_f^{Vac}/k_BT}$ (k_B is Boltzmann constant). The relative defect formation energy of two defects with a defect formation energy of E_{f1}^{Vac} and E_{f2}^{Vac} thus determines the concentration ratio of the two defects as $C_1/C_2\tilde{e}^{(E_2^f-E_1^f)/k_BT}$. In this study, the positive V-vacancy and negative C-vacancy formation energy implies that the carbon vacancy is predominant. At room temperature, the concentration C-vacancy is 1.3×10^{98} times that of the V-vacancy. The V-vacancy concentration is negligible at finite temperatures in crystal VC. Therefore, only the hydrogen trapping sites near the C vacancy are considered in the subsequent calculation, while the V vacancy is ignored.

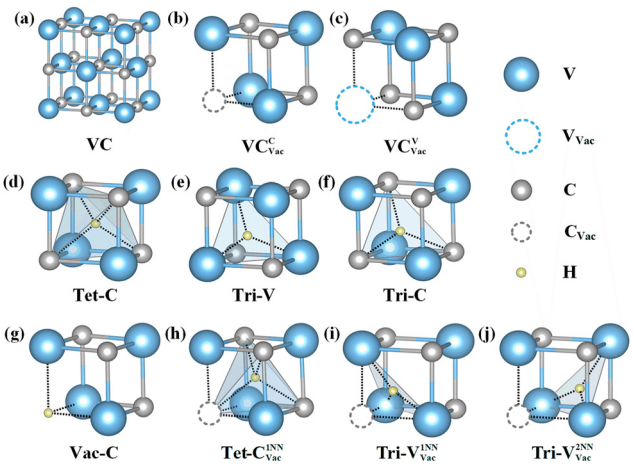

Fig. 1 (a) Crystal structure of VC, (b–c) C vacancy and V vacancy, (d–f) three possible hydrogen trapping sites in VC, and (g–j) four possible hydrogen trapping sites in VC containing a C vacancy.

Table 1 The lattice constant of VC crystal structure, the defect formation energy of vacancies and the H atom solution energy of the trapping sites

Parameters	Unit	Structures	Present work	Ref.
Lattice constant	Å	VC	4.15	4.16,[57] 4.155,[58] 4.161[59]
Defect formation energy	eV	Vac-C	−0.915	−0.880[60]
		Vac-V	4.507	4.365[60]
H atom solution energy	eV	Tet-C	2.215	2.078[19]
		Tri-V	1.750	1.574[19]
		Tri-C	2.213*	2.078[19]
		Vac-C	−0.074	−0.03[29]
		$Tet\text{-}C^{1NN}_{Vac}$	−0.074*	—
		$Tri\text{-}V^{1NN}_{Vac}$	−0.074*	—
		$Tri\text{-}V^{2NN}_{Vac}$	1.489	—

In the VC unit cell, the H atom can occupy three possible interstitial sites, namely the tetrahedral interstitial site where the H atom is equidistant from four C atoms (Tet-C), the trigonal interstitial sites where the H atom lies in a plane of three V or C atoms and it is equidistant from the three V or C atoms (Tri-V or Tri-C). These three configurations are shown in Fig. 1(e and f). The solution energies when the H atom occupies various interstitial sites of VC are also listed in Table 1. It shows that the solution energies are all positive, and the value follows the trend: $0 < E^H(\text{Tri-V}) < E^H(\text{Tet-C}) = E^H(\text{Tri-C})$. The Tri-V site is the most stable site among these interstitial sites due to its lowest H atom solution energy, in line with the literature.[19] Meanwhile, the H atom occupying the Tri-C site will relax to the Tet-C site after optimization so that the H atom cannot be stably trapped at this site. This is the reason that the solution energies of these two sites are similar.

Several configurations of the complex sites, including C vacancy, were constructed to study the interaction of the C vacancy with the H atom that occupies its neighboring sites. The H atoms may occupy four different sites: C vacancy (Vac-C), the first nearest neighbor tetrahedral interstitial site of the C vacancy ($Tet\text{-}C^{1NN}_{Vac}$), and the first ($Tri\text{-}V^{1NN}_{Vac}$) and second ($Tri\text{-}V^{2NN}_{Vac}$) nearest neighbor trigonal interstitial sites of the C vacancy. These configurations are shown in Fig. 1(g–j), and the H atom solution energy of the C vacancy complex site determined using eqn (2) is shown in Table 1. It indicates that the solution energy at the Vac-C site is −0.074 eV, which is similar to the calculated value of −0.03 eV by Ma.[29] In comparison with the Tet-C and Tri-V sites, the H atom solution energy at the Vac-C site is much lower than at these two trapping sites, indicating that the C vacancy has a strong binding effect on the H atom. Due to the influence of the C vacancy, the $Tet\text{-}C^{1NN}_{Vac}$ and $Tri\text{-}V^{1NN}_{Vac}$ sites become unstable, and the H atom will spontaneously move to the C vacancy after atomic relaxation. When the H atom occupies the $Tri\text{-}V^{2NN}_{Vac}$ site with the existence of a C vacancy, the solution energy is 1.489 eV and it can still exist stably at the site after atomic relaxation. Moreover, the H atom solution energy of the $Tri\text{-}V^{2NN}_{Vac}$ site is lower than that of the Tri-V site, indicating that the C vacancy can enhance the hydrogen trapping ability of the interstitial site. The order of the H atom solution energy of four stable hydrogen trapping sites is $E^H(\text{Vac-C}) < 0 < E^H(\text{Tri-}V^{2NN}_{Vac}) < E^H(\text{Tri-V}) < E^H(\text{Tet-C})$.

The chemical and mechanical effects of stable sites are shown in Fig. 2. A different level of lattice distortion occurs when the H atom occupies the trapping site, which causes the mechanical effects of the sites to be positive and weakens the hydrogen trapping ability. Among these four stable sites, only when the H atom occupies the Vac-C site, the mechanical effect is close to zero and the chemical effect is negative, indicating

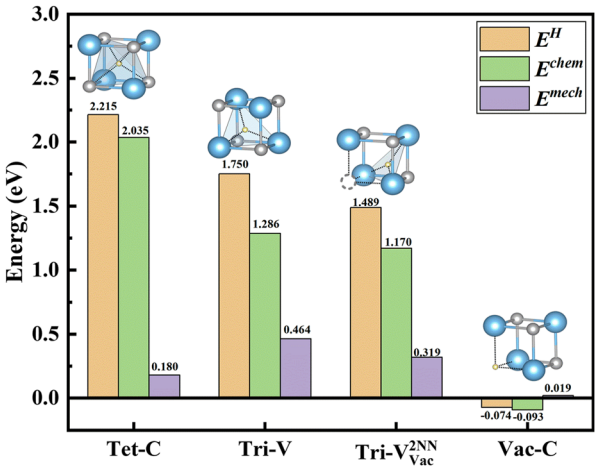

Fig. 2 The H atom solution energy of the four stable hydrogen trapping sites (Tet-C, Tri-V, Tri-V_{Vac}^{2NN}, Vac-C) and their corresponding chemical and mechanical effects.

that the C vacancy has a strong hydrogen trapping ability. In the Tet-C, Tri-V and Tri-V_{Vac}^{2NN} sites, the chemical effects are all positive, and the proportions of H atom solution energy are 91.9%, 73.5% and 78.6%, respectively, indicating that the chemical effect dominates the H atom solution energy. In terms of the mechanical effect, it is lower for the Tet-C site than the Tri-V site since the tetrahedral interstitial volume is larger than the trigonal interstitial volume. However, the H atom is more stable at the Tri-V site due to its lower chemical effect. In the presence of the C vacancy, the H atom solution energy is reduced by 0.261 eV when the H atom occupies the Tri-V_{Vac}^{2NN} sites compared with the Tri-V site without a C vacancy, where the mechanical effect is reduced by 0.145 eV. The reduction in mechanical effect is due to the attraction of the C vacancy, resulting in a slight movement of the H atoms toward the C vacancy, which increases the interstitial volume and reduces the lattice distortion, thereby reducing the H atom solution energy. Therefore, the C vacancy can improve the hydrogen capture ability of the site by reducing the chemical effect and weakening the negative effect of the mechanical effect on the H atom solution energy.

3.2 Thermodynamics stabilities

The structures stability was ensured by the energy minimization during the structure relaxation *via* the conjugate gradient method. We have further examined the thermodynamics stability of these four hydrogen trapping sites *via ab initio* molecular dynamics (AIMD) at the finite temperatures, as shown in Fig. 3. The AIMD simulation was carried out for 5 ps in the *NVT* ensemble at room temperature (300 K) employing Nose–Hoover thermostats, with a time step of 0.0001 ps.

The AIMD results illustrated that the total energy and temperature of these systems converged with fluctuations after 1 ps relaxation, indicating that they have good thermodynamics stabilities.

3.3 Electronic localization function analysis

Among the four stable trapping sites, the stability of the trapping site is closely related to the local chemical environment

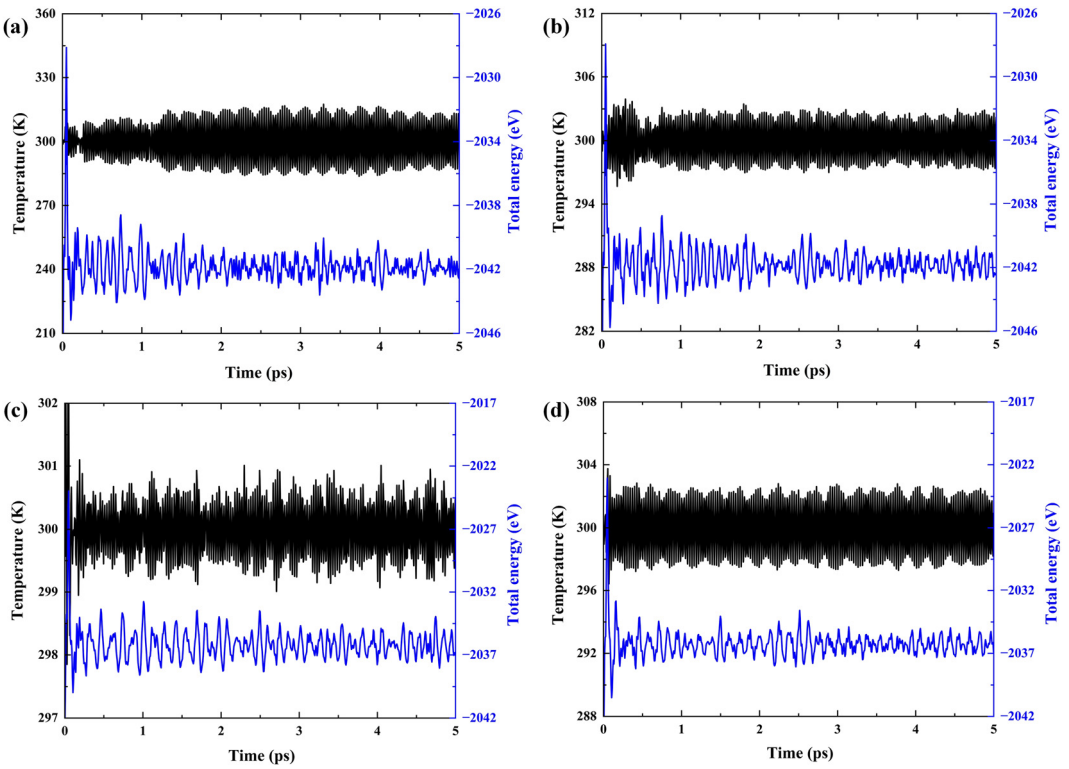

Fig. 3 The temperature (left *Y* axis) and total energy (right *Y* axis) as a function of time in AIMD simulations at 300 K for (a) Tet-C, (b) Tri-V, (c) Tri-V_{Vac}^{2NN}, and (d) Vac-C.

such as charge density, charge transfer and atomic bonding since the chemical effect is the main component of the H atom solution energy. The electron localization function (ELF) is usually used to analyze the spatial localization of the electron charges.[61] By comparing the ELF value £, the relationship between the charge density and the hydrogen capture ability of the site was investigated. The ELF plots of the VC supercell with and without C vacancy before trapping a H atom are shown in Fig. 4(a and b), and the stable hydrogen trapping sites of the two configurations were marked. The ELF value is between 0 and 1, and the values of 0, 0.5 and 1 correspond to vacuum, homogenous electron gas and completely localized state, respectively. Then the ELF values £ of the four hydrogen trapping sites are shown in Fig. 4(c). The order of ELF values at the four sites is £(Tet-C) < £(Tri-V) < £(Tri-V_{Vac}^{2NN}) < £(Vac-C). The ELF value £ at the Vac-C site reaches the maximum value (0.475) and is close to the homogenous electron gas state. The order of ELF values is basically consistent with the variation law of H atom solution energy and chemical effect. This indicates that the H atom trapping behavior in VC conforms to the charge transfer mechanism.[35] The H atom prefers to occupy higher charge density interstitial sites. The higher the degree of localization of the charge density at the trapping site, the easier it is for the H atom to achieve a stable $1s^2$ valence electron structure, resulting in a lower H atom solution energy and chemical effect at the trapping site, and the H atom is more easily dissolved at this site.

3.4 Bader analysis

Bader analysis is the method of determining atomic interaction based on charge density,[62] and the Bader atomic volume defined as the zero-flux surface of charge density can visualize the electronic characteristics in different chemical environments.[63] The relationship between the Bader atomic volume and the solution energy or chemical effect is shown in Fig. 4(d), where the shape of the Bader atomic volume of H atom at various stable trapping sites is included.

The Bader atomic volume of the H atom has a negative linear correlation with the H atom solution energy and its chemical effects. The H atom becomes more stable at the site with the increasing of the Bader atomic volume of the H atom attributed to the lower H atom solution energy. Thus, the Bader atomic volume of the H atom reflects the change of charge transfer in different chemical environments. Moreover, the existence of a C vacancy greatly increases the Bader atomic volume of the H atom at both Vac-C site and Tri-V_{Vac}^{2NN} site, which results in a significant decrease in the H atom solution energy and increases the hydrogen trapping ability of the trapping sites.

3.5 DOS and COHP analysis

Although the DOS is powerful in qualitatively analyzing orbital hybridization and chemical bonding properties, it cannot quantitatively analyze the change in chemical bonding between a H atom and neighboring atoms, especially the weight effect of M−H and C–H bonds on the hydrogen trapping ability of stable sites. While the COHP method can deeply analyze the bonding characteristics between the different atoms, it has been widely used to analyze the interaction between H atoms and neighboring atoms in different systems such as high-entropy alloys and perovskites, providing an important reference for the quantitative study of atomic interactions.[64,65] The PDOS is obtained by integrating the charge density in the reciprocal space, which can characterize the distribution of electrons in an individual orbit, and reflect the hybridization between the electron orbits through the resonance peak. On the other hand, the COHP divides the energy of the band structure into bonding, anti-bonding, and non-bonding contributions, and the bond strength is evaluated based on COHP.

The combination of PDOS and COHP analysis can quantitatively describe the bonding characteristics of H atoms with neighboring atoms, and the results are shown in Fig. 5. Following the convention, the positive value of –COHP represents bond interaction, while the negative value indicates anti-bonding interactions.

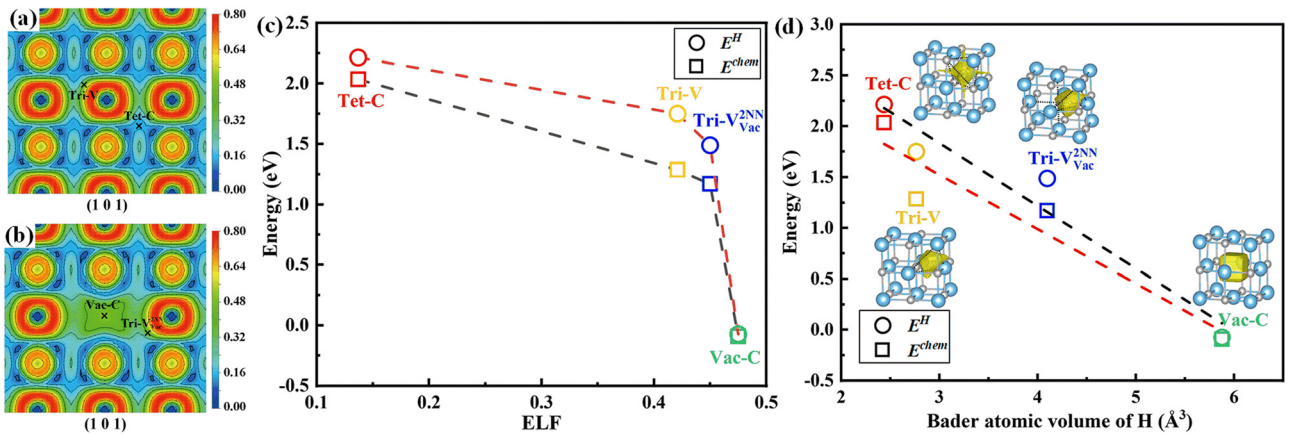

Fig. 4 Electronic localization function (ELF) of the VC (101) surface and four stable hydrogen trapping sites (Tet-C, Tri-V, Tri-V_{Vac}^{2NN}, Vac-C). (a) Without C vacancy and (b) with C vacancy. (c) The ELF value and (d) Bader atomic volume of H at different hydrogen trapping sites as a function of the H atom solution energy and chemical effect.

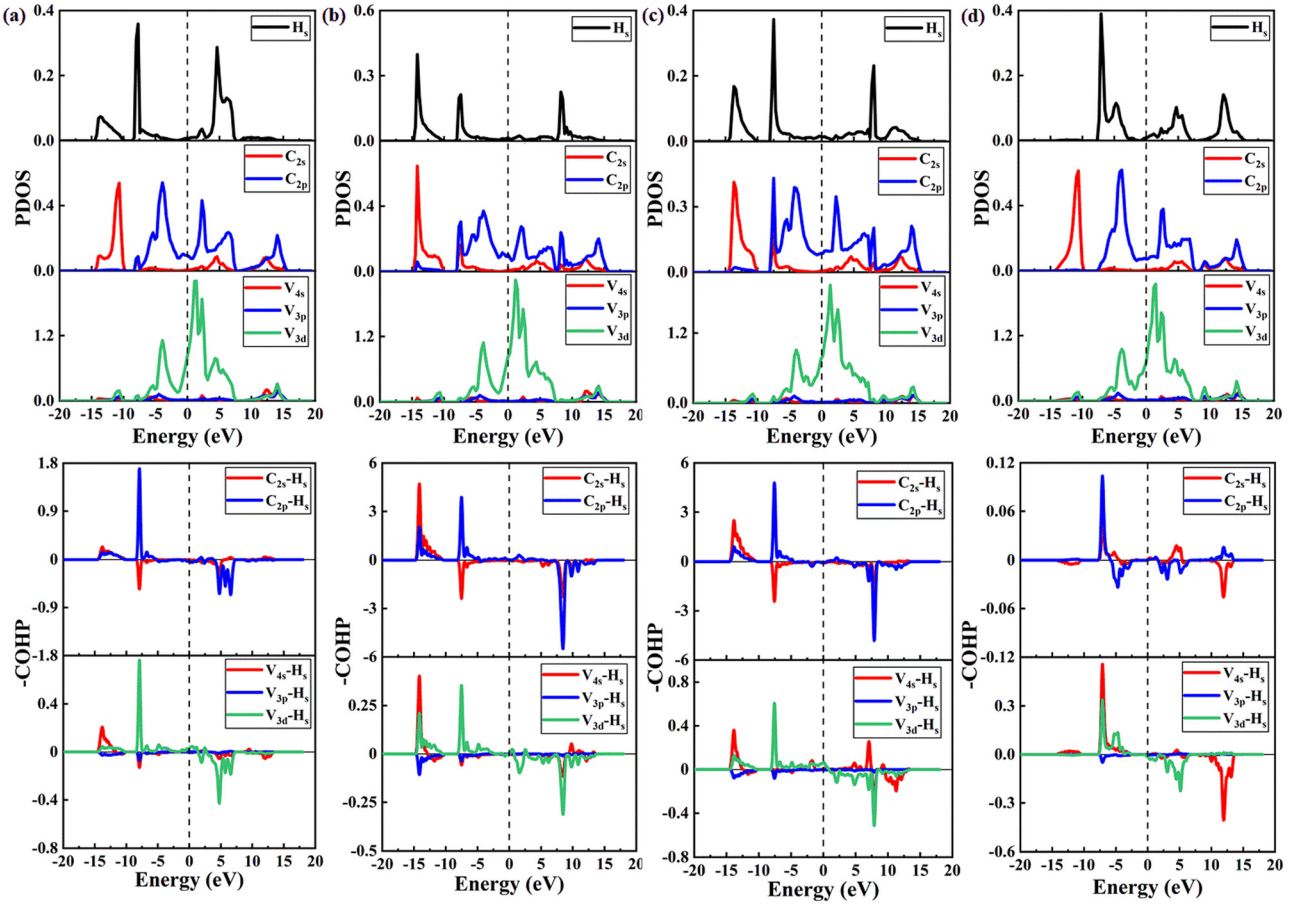

Fig. 5 PDOS of four hydrogen trapping sites and their corresponding COHP analysis. (a) Tet-C, (b) Tri-V, (c) Tri-V_{Vac}^{2NN}, and (d) Vac-C. The dotted line at 0 eV is the position of the Fermi level.

When the H atoms occupy the tetrahedral and trigonal interstitial sites (Tet-C, Tri-V and Tri-V_{Vac}^{2NN}), the H_s, C_{2s} and V_{4s} orbitals hybridize at −14 eV. A weak resonance peak forms at the Tet-C site, while sharp resonance peaks form at the Tri-V and Tri-V_{Vac}^{2NN} sites. At -8 eV, strong hybridization occurs in the H_s, C_{2p} and V_{3d} orbitals of these configurations, indicating that strong covalent bonds are formed between them. The resonance peaks above the Fermi level are mainly anti-bonding orbital positions generated by the hybridization of H atoms with adjacent atoms. There are no electrons at these orbitals, which is beneficial to the reduction of system energy.

3.6 ICOHP analysis

The ICOHP analysis of orbital bonding strength in the three configurations of Tet-C, Tri-V and Tri-V_{Vac}^{2NN} is shown in Fig. 6. The integral of crystal orbital Hamilton populations (ICOHP) is obtained by integrating the part of the COHP below the Fermi level, which can be used to measure the strength of covalent bonds in the crystal. The lower the value is, the stronger the bond there will be.[66–68] There are mainly V–H and C–H bonds between the H atom and the neighboring atoms. Among them, C–H bonds account for a dominant proportion, 63.3%, 91.8%, and 81.3%, respectively, indicating that the C–H bond makes the main contribution to the bonding between the H atom and

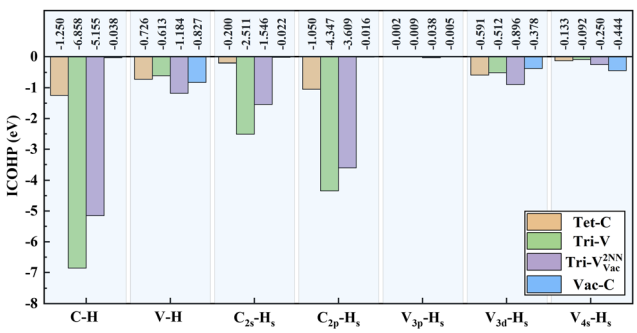

Fig. 6 The ICOHP value of C–H and V–H bonds for the various orbitals of the four stable hydrogen trapping sites (Tet-C, Tri-V, Tri-V_{Vac}^{2NN}, Vac-C).

its neighboring atoms. The length of the C–H bond in these three configurations is 1.795 Å, 1.153 Å, and 1.262 Å, while the V–H bond length is 1.878 Å, 1.849 Å, and 1.731 Å, respectively. Among the C–H bonds, there are C_{2p}–H_s and C_{2s}–H_s bonds, mainly dominated by C_{2p}–H_s bonds and the strength of C_{2s}–H_s bonds accounts for less than 36.6%. This is mainly due to the existence of anti-bonding orbitals below the Fermi level in the C_{2s}–H_s bond, which weakens the strength of the C_{2s}–H_s bond. There are V_{3d}–H_s and V_{4s}–H_s bonds in the V–H bond. Among them, the strength of V3d–Hs accounts for more than 75.7%,

serving as the main contribution of the V–H bond. Therefore, the main contribution to the chemical effect when hydrogen atoms occupy the Tet-C, Tri-V and Tri-V_{Vac}^{2NN} sites comes from the C-H bond formed by C_{2p}–H_s orbital hybridization and the V–H bond formed by V_{3d}–H_s orbital hybridization.

When the H atom occupies a C vacancy (Vac-C), the ICOHP analysis of the bond strength is also shown in Fig. 6. The distance between the H atom and neighboring C and V atoms is 2.913 Å and 2.181 Å, respectively. Due to the large separation between the H atom and the C atom, there is basically no hybridization between them. In this scenario, the H atom mainly forms a V–H bond with V atoms, and correspondingly the V–H bond accounted for 95.6%. Below the Fermi level, the H_s and V_{3d}, V_{4s} orbitals hybridize only at −7 eV. There are V_{3d}–H_s and V_{4s}–H_s bonds in the V–H bond through ICOHP analysis, with the weight of 45.7% and 53.7%, respectively. Thus, the V_{4s}-H_s bond, unlike other stable trapping sites, is the main contribution of the V–H bond, mainly due to the changes in the bonding level and antibonding orbital. In this respect, the main contribution of the chemical effect comes from the V–H bond formed by the V_{4s}–H_s hybridization when the H atom occupies the Vac-C site.

When the H atom occupies the Vac-C site, there is only a V–H bond with a strength larger than that of other sites without C vacancy, and the H atom solution energy is the lowest. When H atoms occupy the Tri-V and Tri-V_{Vac}^{2NN} sites, the attraction of the C vacancy weakens the strength of the C–H bond and increases the strength of the V–H bond. Because the existence of the C vacancy enhances the hydrogen trapping ability of the trapping site, the H atom solution energy and chemical effect of the Tri-V_{Vac}^{2NN} site are lower than those of the Tri-V site. Therefore, the C vacancy may enhance the hydrogen trapping ability of the trapping site by increasing the strength of the V–H bonds. When H atoms occupy the Tet-C and Tri-V sites, the C–H bond strength of the Tri-V site is six times stronger than that of the Tet-C site. However, the C–H bond length of the Tri-V site is only 0.598 Å shorter than that of the Tet-C site, owing to the stronger hybridization of the H_s and C_{2s} orbitals at the Tri-V site. The strong C–H bond may also be responsible for the stronger hydrogen trapping ability of the Tri-V site.

The question of why the H atom cannot stably exist at the Tet-C_{Vac}^{1NN} and Tri-V_{Vac}^{1NN} sites can be explained by the inability to form a strong C–H bond between H and the neighboring C atom. In addition, the strong C–H bond resists the attraction of the C vacancy. Thus, it can be concluded that the strength of the C–H bond determines the hydrogen trapping ability of the trapping site in the absence of a C vacancy. The strength of the V–H bond increases in the presence of a C vacancy, which favors hydrogen trapping. Furthermore, the C vacancy can affect the hydrogen trapping ability of trapping sites in different chemical environments by changing the proportion of the bonding strength to the total strength of each hybrid.

With the acknowledgment of the hydrogen trapping capabilities of the individual atomic structures, the hydrogen trapping capabilities could be optimized and controlled. With defect engineering, the presence, concentration, and atomic configuration of the C vacancy have promising applications in the material design of hydrogen permeation barrier coatings. It is worth noting that these defects could be the passive products of radiation damage[69] during the operation of the reactors. Therefore, the structure and concentration are dynamics, as a function of the irradiation. Combined with the fluence and the operation condition, the intake of hydrogen could be further predicted, which is helpful in the safety monitoring and other more practical functions.

Conclusions

The hydrogen atom solution energy of trapping sites in vanadium carbides, including C vacancy neighboring sites, has been investigated by first-principles calculations. A detailed electronic structure analysis has been carried out for insights into the chemical environment effects. The main results of the study are summarized as follows.

The H atom solution energy mainly depends on the chemical effect. When a C vacancy exists, the hydrogen trapping ability of the stable site will be improved by reducing the chemical effect and weakening the negative effect of the mechanical effect on the H atom solution energy.

The hydrogen trapping ability of the stable site is closely related to the local chemical environment such as charge density, charge transfer and atomic bonding. The H atom tends to occupy the site with the higher charge density, and the Bader atomic volume of the H atom can be used to describe the H atom solution energy of the trapping sites in VC. In addition, the C vacancy increases the charge density and the Bader atomic volume of the H atom at the trapping site, which leads to a significant reduction in H atom solution energy and increases the hydrogen trapping ability of the stable site.

The strength of the C–H bond determines the hydrogen trapping ability of the trapping site in the absence of a C vacancy. When a C vacancy exists, the increase in V–H bond strength may be the reason for the enhanced trapping ability of the trapping site. Thus, the C vacancy affects the hydrogen trapping ability of the trapping sites in different chemical environments by changing the proportion of the bonding strength to the total strength of each hybrid orbital.

Our electronic structure analysis and insights into the atomic structures of the hydrogen-vacancy-interstitial complex in vanadium carbide suggest the defect engineering to optimize the hydrogen trapping for coatings. Our results could provide research ideas for the aggregation and trapping of multiple H near multiple vacancies, laying the foundation for material design and safety monitoring of the next hydrogen permeation barrier coatings.

Conflicts of interest

There are no conflicts to declare.

Acknowledgements

S. T. gratefully acknowledges the financial support from NSFC (No. 52175293 and 51774083), and Q. P. would like to

acknowledge the support provided by the LiYing Program of the Institute of Mechanics, Chinese Academy of Sciences (No. E1Z1011001). The authors acknowledge the Fundamental Research Funds for the Central Universities (No. N2007002 and N2007011) and 111 Project (Grant No. B20029).

References

1 D. Terentyev, A. Puype and O. Kachko, *Nucl. Mater. Energy*, 2021, **29**, 101070.
2 T. Muroga, T. Nagasaka and K. Abe, *J. Nucl. Mater.*, 2002, **307**, 547–554.
3 J. Chen, S. Qiu, Y. Lin, Z. Xu and Y. Xu, *J. Nucl. Mater.*, 2002, **302**, 135–142.
4 J. R. Distefano, J. Van, D. H. Röhrig and L. D. Chitwood, *J. Nucl. Mater.*, 1999, 102–110.
5 Q. Peng, G. Lu and Y. Sun, *Phys. Rev. B: Condens. Matter Mater. Phys.*, 2013, **88**, 104109.
6 Z. Zhang, Z. Yang, S. Lu, A. Harte, R. Morana and M. Preuss, *Nat. Commun.*, 2020, **11**, 4890.
7 J. P. Hanson, A. Bagri and J. Lind, *Nat. Commun.*, 2018, **9**, 3386.
8 N. Takano, *Mater. Sci. Eng., A*, 2008, **483**, 336–339.
9 J. Song and W. A. Curtin, *Nat. Mater.*, 2013, **12**, 145–151.
10 D. H. Lassila and H. K. Birnbaum, *Acta Metall.*, 1986, **34**, 1237–1243.
11 S. Li, D. He, X. Liu, S. Wang and L. Jiang, *J. Nucl. Mater.*, 2012, **420**, 405–408.
12 Y. Wu, S. Zhu and Y. Zhang, *Int. J. Hydrogen Energy*, 2016, **41**, 10827–10832.
13 L. Wu, T. Yao, Y. Wang, J. Zhang, F. Xiao and B. Liao, *J. Alloys Compd.*, 2013, **548**, 60–64.
14 Y. Ren, L. Li, Y. Zhou and S. Wang, *Mater. Lett.*, 2022, **315**, 131962.
15 Y. Liu, S. Huang, J. Ding, Y. Yang and J. Zhao, *Int. J. Hydrogen Energy*, 2019, **44**, 6093–6102.
16 H. Liu, H. Zhou, G. Luo and P. Zheng, *J. Nucl. Mater.*, 2021, **554**, 153071.
17 T. Depover and K. Verbeken, *Mater. Sci. Eng., A*, 2016, **675**, 299–313.
18 H. J. Seo, J. N. Kim, J. W. Jo and C. S. Lee, *Int. J. Hydrogen Energ.*, 2021, **46**, 19670–19681.
19 Y. Li, X. Zhang and T. Wu, *Int. J. Hydrogen Energy*, 2021, **46**, 22030–22039.
20 L. Li, B. Song and Z. Cai, *Mater. Sci. Eng., A*, 2019, **742**, 712–721.
21 Y. Lin, H. Yi, Z. Chang, H. Lin and H. Yen, *Front. Mater.*, 2021, **7**, 611390.
22 Y. Chen, H. Lu and J. Liang, *Science*, 2020, **367**, 171–175.
23 W. Y. Choo and J. Y. Lee, *Metall. Trans. A*, 1982, **13**, 135–140.
24 M. Koyama, M. Rohwerder and C. C. Tasan, *Mater. Sci. Technol.*, 2017, **33**, 1481–1496.
25 G. K. Gueorguiev, Z. Czigány and A. Furlan, *Chem. Phys. Lett.*, 2011, **501**, 400–403.
26 A. Kakanakova-Georgieva, G. K. Gueorguiev and D. G. Sangiovanni, *Nanoscale*, 2020, **12**, 19470–19476.
27 Y. He, Y. Su, H. Yu and C. Chen, *Int. J. Hydrogen Energy*, 2021, **46**, 7589–7600.
28 X. Kong, S. Wang and X. Wu, *Acta Mater.*, 2015, **84**, 426–435.
29 Y. Ma, Y. Shi and H. Wang, *Int. J. Hydrogen Energy*, 2020, **45**, 27941–27949.
30 J. Takahashi, K. Kawakami and T. Tarui, *Scr. Mater.*, 2012, **67**, 213–216.
31 X. Yu, G. B. Thompson and C. R. Weinberger, *J. Eur. Ceram. Soc.*, 2015, **35**, 95–103.
32 W. S. Williams, *Mater. Sci. Eng., A*, 1988, **105–106**, 1–10.
33 J. Takahashi, K. Kawakami and Y. Kobayashi, *Acta Mater.*, 2018, **153**, 193–204.
34 S. Echeverri Restrepo, D. Di Stefano and M. Mrovec, *Int. J. Hydrogen Energy*, 2020, **45**, 2382–2389.
35 W. Xing, X. Chen, Q. Xie, G. Lu, D. Li and Y. Li, *Int. J. Hydrogen Energy*, 2014, **39**, 11321–11327.
36 Y. Liu, Y. Zhang and H. Zhou, *Phys. Rev. B: Condens. Matter Mater. Phys.*, 2009, **79**, 172103.
37 Z. Su, S. Wang, C. Lu and Q. Peng, *Materials*, 2020, **13**, 322.
38 R. L. Liu and D. Y. Li, *Scr. Mater.*, 2021, **204**, 114148.
39 X. Tao, H. Chen, Y. Zhou, Q. Peng and Y. Ouyang, *J. Nucl. Mater.*, 2021, **557**, 153235.
40 X. Wang, C. Xu, S. Hu, H. Zhang, X. Zhou and S. Peng, *J. Nucl. Mater.*, 2019, **521**, 146–154.
41 X. Yang, Y. Lu and P. Zhang, *J. Nucl. Mater.*, 2016, **479**, 130–136.
42 S. Huang, J. Tian and Y. Liu, *J. Nucl. Mater.*, 2021, **554**, 153096.
43 G. Kresse and J. Furthmüller, *Comput. Mater. Sci.*, 1996, **6**, 15–50.
44 P. E. Blöchl, *Phys. Rev. B: Condens. Matter Mater. Phys.*, 1994, **50**, 17953–17979.
45 J. P. Perdew, J. A. Chevary and S. H. Vosko, *Phys. Rev. B: Condens. Matter Mater. Phys.*, 1993, **48**, 4978.
46 J. P. Perdew, K. Burke and M. Ernzerhof, *Phys. Rev. Lett.*, 1996, **77**, 3865–3868.
47 D. J. Chadi, *Phys. Rev. B: Condens. Matter Mater. Phys.*, 1977, **16**, 1746–1747.
48 K. Ohsawa, K. Eguchi and H. Watanabe, *Phys. Rev. B: Condens. Matter Mater. Phys.*, 2012, **85**, 94102.
49 K. Momma and F. Izumi, *J. Appl. Crystallogr.*, 2011, **44**, 1272–1276.
50 W. Tang, E. Sanville and G. Henkelman, *J. Phys.: Condens. Matter*, 2009, **21**, 84204.
51 V. L. Deringer, A. L. Tchougreeff and R. Dronskowski, *J. Phys. Chem. A*, 2011, **115**, 5461–5466.
52 O. I. Gorbatov, A. H. Delandar and Y. N. Gornostyrev, *J. Nucl. Mater.*, 2016, **475**, 140–148.
53 B. He, W. Xiao, W. Hao and Z. Tian, *J. Nucl. Mater.*, 2013, **441**, 301–305.
54 U. Aydin, L. Ismer, T. Hickel and J. Neugebauer, *Phys. Rev. B: Condens. Matter Mater. Phys.*, 2012, **85**, 155144.
55 H. Sawada and T. Omura, *Comput. Mater. Sci.*, 2021, **198**, 110652.
56 Y. He, Y. Su, H. Yu and C. Chen, *Int. J. Hydrogen Energy*, 2021, **46**, 7589–7600.
57 E. I. Isaev, R. Ahuja and S. I. Simak, *Phys. Rev. B: Condens. Matter Mater. Phys.*, 2005, **72**, 64515.

58 J. Ding, D. Sun and Y. Yang, *Nucl. Instrum. Methods Phys. Res., Sect. B*, 2020, **479**, 163–170.
59 Z. Sun, R. Ahuja and J. E. Lowther, *Solid State Commun.*, 2010, **150**, 697–700.
60 J. Guo, Y. Feng, C. Tang and X. Ren, *J. Am. Ceram. Soc.*, 2020, **103**, 7226–7239.
61 Q. Peng and S. De, *Phys. E*, 2012, **44**, 1662–1666.
62 G. Henkelman, A. Arnaldsson and H. Jónsson, *Comp. Mater. Sci.*, 2006, **36**, 354–360.
63 B. Zhang, J. Su and M. Wang, *Acta Mater.*, 2021, **208**, 116744.
64 Z. Xie, Y. Wang, C. Lu and L. Dai, *Mater. Today Commun.*, 2021, **26**, 101902.
65 L. Xu and D. Jiang, *Comp. Mater. Sci.*, 2020, **174**, 109461.
66 Harshit, N. Roy, A. Chakrabarty and P. P. Jana, *Solid State Sci.*, 2021, **113**, 106544.
67 M. Ren, X. Guo and S. Huang, *Appl. Surf. Sci.*, 2021, **556**, 149801.
68 J. Wang, M. Enomoto and C. Shang, *Acta Mater.*, 2021, **219**, 117260.
69 Q. Peng, F. Meng and Y. Yang, *Nat. Commun.*, 2018, **9**, 4880.

